Atom Indonesia

Journal homepage: http://aij.batan.go.id

The Effect of Sr^{2+} and Fe^{3+} Cations and the Stirring Speed on The Precipitation of Barium Sulfate in a Batch System

S. Susilowati[1,2*], N. Karaman[1,2], A. R. Prayuga[2], D. T. Aruba[2], Sukirmiyadi[1], L. Suprianti[2]

[1]*Master of Environmental Science, Engineering Faculty, University of Pembangunan Nasional "Veteran" East Java, Surabaya, 60294, Indonesia*

[2]*Department of Chemical Engineering, Engineering Faculty, University of Pembangunan Nasional "Veteran" East Java, Surabaya, 60294, Indonesia*

ARTICLE INFO

Article history:
Received 16 June 2023
Received in revised form 2 October 202
Accepted 2 October 2023

Keywords:
Barium sulfate
Batch system
Cation
Precipitation rate

ABSTRACT

The batch system investigation explored the effect of Sr^{2+} and Fe^{3+} cations and the stirring speed on the characteristics of precipitated barium sulfate. A series of experiments were conducted to evaluate the rate of barium sulfate precipitation in laboratory equipment from brines containing barium ions (3500 ppm) and varying amounts of Sr^{2+} and Fe^{3+} ions (10 and 20 ppm). Kinetic analysis was also performed to explore how stirring speeds (240 and 480 rpm) affect barium sulfate scales' crystallization by increasing the stirring speed and promoting Sr^{2+} and Fe^{3+}-cation solubility while decreasing the precipitation rate. All solid crystals obtained were mostly pure barite, as the X-ray diffraction (XRD) method confirmed. The SEM micrograph of barite morphology revealed particles with tablet-shaped crystals 2 to 5 nm in size. With the presence of Sr^{2+} and Fe^{3+}-cation, the shape of barium sulfate was modified into spherical tablets or flower-like clusters of tablets. Meanwhile, the morphological changes could result from increased stirring rates. Moreover, the kinetic results yielded a general reaction rate equation that might be used to estimate barium sulfate deposition in pipelines for various brine, supersaturation, and mixing time durations.

INTRODUCTION

Scale formation on pipelines and industrial equipment substantially impacts oil production performance in the oil industry. Scaling can occur in down-hole or surface facilities, impeding fluid flow. Scaling is a particularly unwanted crystallization on the metal surface of equipment because its formation can result in a range of unwanted results, including loss of output, decrease of product purity, and maintenance difficulties, to name a few [1]. Furthermore, equipment damage and disruptions, a loss in injectivity of injection wells, and a significant fall in oil production rate are all common in this regard [2-4]. Combining incompatible injection water with changing ion concentrations at high pressure (> 69 MPa) and temperature (>150 °C) circumstances might result in the development of sulfate salts, which are essential components of scale [5]. Due to water incompatibility, certain sulfate scales, such as calcium, barium, and strontium sulfate, may influence oil production by increasing the water required [6-8]. Scale can be formed by either induced crystallization or alternative crystallization mechanisms, typically associated with heterogeneous nucleation [9,10]. Oil field scaling is mainly caused by mixing incompatible waters, which occurs when two liquids chemically interact, resulting in mineral precipitation during mixing. Incompatible waters include seawater with high SO_4^{-2} concentrations but low Ca^{+2}, and Ba^{+2}/Sr^{+2} concentrations and formation waters with very low SO_4^{-2} concentrations but high Ca^{+2}, Ba^{+2}, and Sr^{+2} concentrations [11]. The precipitation of $CaSO_4$, $BaSO_4$, and $SrSO_4$ was caused by mixing the liquids [12]. Field water (disposal water) may also be incompatible with the ocean [13,14]. The scale can form when wastewater is mixed with seawater for re-injection [15]. Scaling can occur in nuclear

*Corresponding author.
E-mail address: susilowati.tk@upnjatim.ac.id
DOI: https://doi.org/10.55981/aij.2023.1341

desalination when there is a high concentration of salts and minerals in the feed water. This can lead to the formation of scale on the heat transfer surfaces of the desalination unit, reducing its efficiency and potentially causing damage. To prevent scale formation, anti-scalants can be added to the feed water, or the water can be pre-treated to remove scale-forming ions [16].

Another type of fluid incompatibility is the sulfide scale, formed when hydrogen sulfide gas reacts with iron, zinc, or lead-rich formation fluids [17]. Salt precipitation occurs when salt concentrations rise over the solubility limit due to brine evaporation. Dehydration and, more typically, NaCl precipitation occurs when a dry gas stream mixes with a low-rate brine stream in a high-pressure/high-temperature gas well. Furthermore, Fe^{3+} (and Fe^{2+}) ions can co-precipitate with barium sulfate [18], resulting in a precipitate with physical and chemical characteristics distinct from the pure precipitate. Adsorption mechanisms are usually thought to be how Fe^{3+} co-precipitates with barium sulfate [11].

Furthermore, batch system experiments looked into the impact of co-precipitated Sr^{2+} and Fe^{3+} cations on the physical properties of barium sulfate crystals since the adsorption processes differed [19]. As a result, the effects of Sr^{2+} and Fe^{3+}-cations on the physical characteristics of barium sulfate may be less significant in terms of addiction because they both have almost the same ionic radius for developing the crystal structure. Furthermore, the Sr^{2+} cation may affect the volume of the barium sulfate crystal through ion replacement because their ionic radii might be compared. On the other hand, Fe^{3+}-cation might be absorbed into its crystal lattice and significantly modify the properties of the succeeding precipitate due to its structural changes in the crystal [20,21].

Despite extensive research dealing with the effects of strontium and ferric iron on barium sulfate crystallization, fundamental issues about their effects on scale formation in a simple laboratory system, regardless of promotion or inhibition, had not been yet studied. This study aimed to find strontium and ferric iron cations in synthetic brine on barium sulfate precipitation. Meanwhile, the effects of strontium and ferric iron concentrations by stirring on the speed of morphology and deposition rates had already been specifically investigated. Moreover, the aqueous crystallization system's alteration in mineralogy and morphology was investigated by using XRD (X-ray diffraction) and SEM examination. XRD is used to determine the crystal structure of a material. It can reveal the arrangement of atoms or ions within a crystal lattice, including unit cell parameters, atomic positions, and crystal symmetry. This information is crucial for understanding the physical and chemical properties of a material. Therefore, this crystallization experiment aimed to forecast the overall barium sulfate crystallization trend in the water reservoir.

METHODOLOGY

Research method

Analytical grade powders $BaCl_2$, Na_2SO_4, $SrCl_2$, and $FeCl_3$ (Merck, Germany) were dissolved in distilled water, which was used to implement this study. While barium sulfate was synthesized by implementing Eq. (1).

$$BaCl_{2(aq)} + Na_2SO_{4(aq)} \rightarrow BaSO_{4(salt)} + 2NaCl_{aq} \quad (1)$$

In each experiment, 31.165 g of $BaCl_2$ solid and 18.1 g of Na_2SO_4 were dissolved in 5 L of water to achieve barium and sulfate concentrations at 3500 ppm. Subsequently, two different brines (designated as Brines 1 and 2) were set up for each experiment, each containing varying concentrations of strontium or iron (III). To create solutions with strontium concentrations of 10 ppm and 20 ppm, 0.195 g and 0.39 g of $SrCl_2$ solids were dissolved in 1000 ml of water, respectively. Similarly, for iron (III), 0.135 g and 0.275 g of $FeCl_3$ were suspended in 1000 ml of water to prepare solution concentrations of 10 ppm and 20 ppm.

Each 100 ml of barium and sulfate ions was dripped from the burette into the flask. Then, the stirring temperature (30 °C) and speed (240 and 480 rpm) were adjusted. After that, the magnetic stirrer was turned on, and the brine-rich solution was mixed; for each experiment, the mass of barium crystal product was obtained every 30 minutes for kinetic studies, and the experiment lasted 120 minutes. Sr concentrations were added independently in the experiments for brines 1 (BS1-Sr0, BS1-Sr10, and BS1-Sr20). Likewise, BS2-Fe0, BS2-Fe10, and BS2-Fe20 brine (BS2) samples were generated from barium sulfate with Fe-cations of 0, 10, and 20 ppm. All barium sulfate scales were strained through a 0.45 m paper filter at the end of the tests. The resultant solid scales were then dried in an oven at 100 °C for 24 hours before being weighed for the deposition mass rate estimation. Then, scale samples from each experiment were taken for XRD and SEM examination to examine the crystal and morphological structures of the scales.

Kinetic analysis

The kinetics of barium sulfate precipitation with varied stirring rates were studied using a first-order process as implied in Eq. (2).

$$A \rightarrow \text{Product} \quad (2)$$

When changes in concentration and time were taken into account, the kinetic rate equation could be stated as described in Eq. (3).

$$\text{Rate}(Ms^{-1}) = -\frac{d[A]}{dt} = k[A] \quad (3)$$

By integrating the reaction form, the reaction equation was simply given as shown in Eqs. (4) and (5).

$$\int_{[A]_o}^{[A]} \frac{d[A]}{[A]} = -k \int_0^t dt \quad (4)$$

$$\ln \frac{[A]}{[A]o} = -k * t \quad (5)$$

In this case, [A]o represents the initial concentration of species at time $t = 0$, whereas [A] equals [A]o at time $t = t$,. Using this equation, a straight-line plot of k*t versus ln [A] could be used to determine the reaction kinetics constant for $BaSO_4$ precipitation The chemical raction equation of $BaSO_4$ precipitation is shown at Eq. (6).

$$Ba^{2+} + SO_4^{2-} \rightarrow BaSO_4 \quad (6)$$

Here, [A] denotes the molar concentration of [Ba^{2+}].

Characterization

All precipitated brined samples were analyzed using the XRD (X-ray diffraction) method, with data obtained using an X-ray diffractometer (Bragg Brentano mode- Philips; PW 3050/60). In this measurement, Cu-K radiation settings (=1.5406) were set up for 10-600 2 scans, 0.020 steps, and 0.5 s/step. Meanwhile, the QualX search-match algorithm [22] was used to identify the phase of the minerals scale. Then, the previously discovered phases were validated using XRD Rietveld analysis (Program Fullprof-2k, version 3.30) [23]. The crystal structure model on the COD (Crystallography Open Database) [24] was used to run the XRD Rietveld refinements. The XRD Rietveld refining strategy had already been discussed elsewhere [25]. Instead, the SEM/EDX (JEOL JSM 5200) method was employed for morphological analysis of micrographs collected below 20.0 kV and 1.0 nA experimental circumstances. Furthermore, the previous study, dealing with the analyzed powders, was glued to the surface of the metallic sample holder and then coated with gold.

Statistical analysis

The mean and standard deviation were reported and One Way Analysis of Variance (ANOVA) statistical testing was performed for all chemical parameters to compare the significancy of the variable.

RESULTS AND DISCUSSION

The effect of the presence of the inhibitor on the precipitation rate

This experiment applied two varians of additives (Sr^{2+} and Fe^{3+}) with three variation in concentration (0, 10, 20 ppm). Figure 1 presents the variation of the additive variation as research parameters and mass of the scale barium sulphate formed. The addition of additive has been found to inhibit the crystallization of barium sulphate. the Barite scale decrease by increasing the additive concentration. This is because the Sr^{2+} and Fe^{3+} ion retard the crystal become large enough to precipitate in the solution. The use of Sr^{2+} and Fe^{3+} ion may effective applied for barite scale prevention. This result reasonably well with the previous study where the citric acid mitigate the barite scale formation. By addition the citric acid additive, the barite crystals precipitated showed a star-like crystal with almost similar size [26]. The study also found that the presence of calcium ions can influence the formation of struvite. Research indicates that calcium ions can compete with magnesium in the formation of struvite, resulting in a smaller proportion of struvite[27].

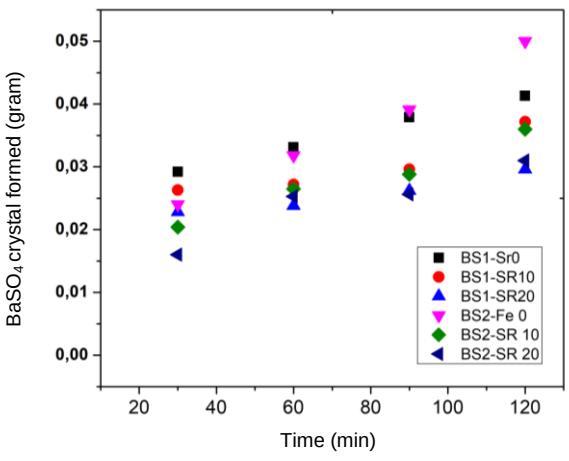

Fig. 1. The effect of additive on barium sulfate scale formation.

The effect of the stirring rate on the barium sulfate crystallization

The experiment was carried out at stirring speed of 240 and 480 rpm. The effect of the stirring speed on the barium sulfate formation as shown at Fig. 2**.** From the experimental result, the stirring rate influences the crystallization process, where the stirring speed of 480 rpm exhibit more barium sulfate crystal. Stirring can enhance mass and heat transfer rates, which are crucial in crystallization processes. It can also affect the size and morphology of the crystals. In this research, the stirring process carried out accelerates the reaction between Ba^{2+} ions and SO_4^{2-} ions, thereby speeding up the formation of barium sulfate crystals. As a result, it was found that stirring at 480 rpm produces a larger quantity of crystal products. in this experiment, the stirring process affect the nucleation. The mechanism is through the contact between one crystal and another through the stirring process. It is called secondary nucleation, when the nucleation is generated from seed crystals in the solution. The size of the crystal nucleus affects secondary nucleation. For example, large crystal nuclei produce larger nuclei in an agitated system than small ones due to the higher probability of contact and collision energy. [28]**.**

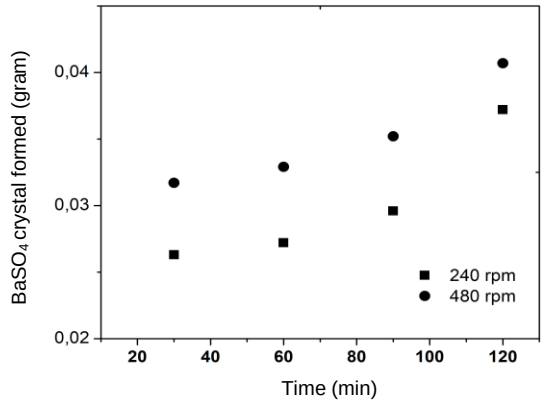

Fig. 2. The effect of stirring rate on scale formation for sampel BS1-SR10.

Kinetic result

In each kinetic analysis experiment, a solution concentration of Ba^{2+} (3500 ppm) and additions of Sr and Fe-ions in amounts of 0, 10, and 20 ppm were studied for varied stirring speeds (240 and 480 rpm). The experimental results revealed the anticipated trend of $BaSO_4$ precipitation by increasing its time duration and stirring speed (Figs. 1 and 2). As a result, the crystallization kinetics of brines were estimated as either the rate of Ba^{2+} reduction or the rate of time increment shown in Figs. 3 and 4.

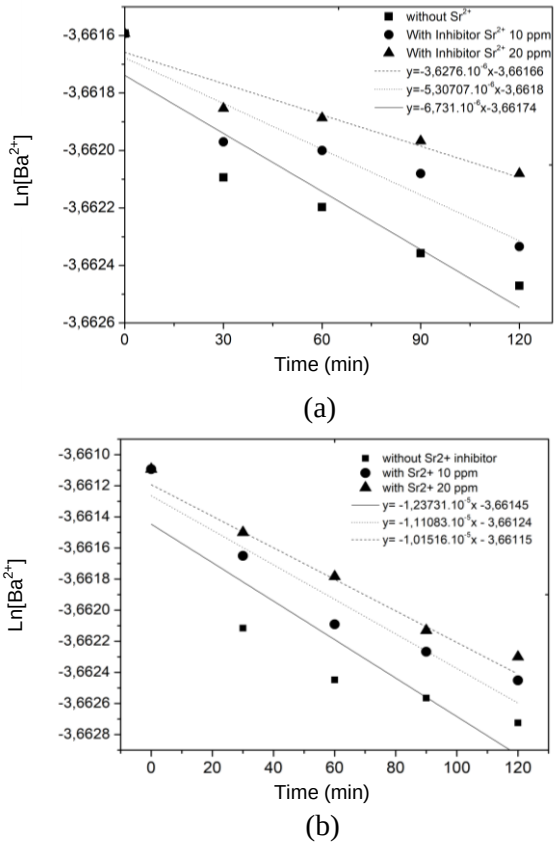

Fig. 3. First-order kinetics of barium sulfate crystallization (BS1-sample) in the absence and presence of Sr^{2+}additives and at a stirring (a) 240 rpm (b) 480 rpm.

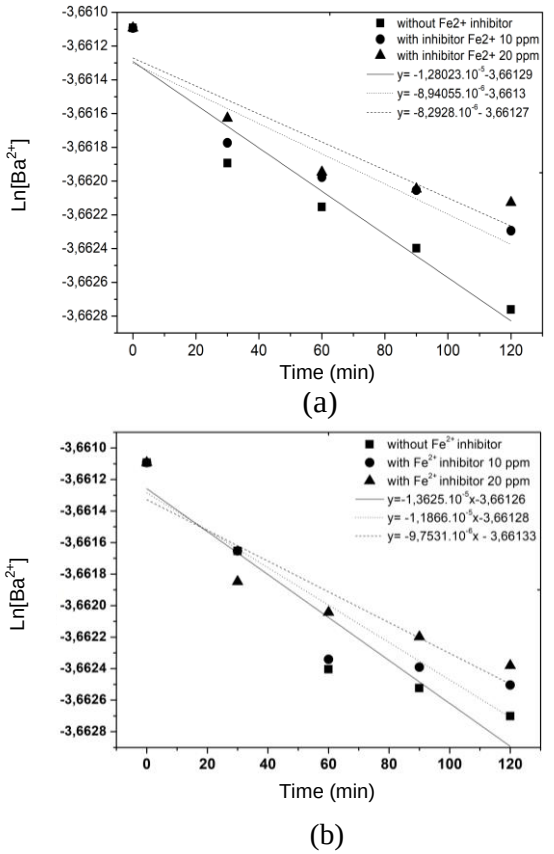

Fig. 4. First-order kinetics of barium sulfate crystallization (BS2-sample) in the absence and presence of Fe^{3+}additives and at a stirring speed of (a) 240 rpm (b) 480 rpm.

Furthermore, kinetic analysis of the BS0 sample revealed the best line of fit for the typical data in the absence of additives. As the first-order kinetics, a correlation coefficient (R^2) of 0,97889 might be used to predict the precipitation rate of a barium sulfate crystal. Furthermore, additional types of brine kinetic (BS-Sr and BS-Fe) followed the crystallization first-order reaction rates. The slopes of the straight lines in Table 1 could be used to investigate the adsorption rate constants (k) of BS-Sr samples.

Table 1. Reaction rate constants for barium sulfate crystallization with Sr^{2+} cations.

Brines with Sr^{2+} (ppm)	Stirring rate (rpm)	Regression	Rate constant (k, min^{-1})	R^2
BS1-Sr0 (0)	240	$y=-6.7310\times\times10^{-6}x$ -3.66174	-6.7310×10^{-6}	0.87428
BS1-Sr0 (0)	480	$y= -1..2373\times10^{-5}x$ -3.66145	-1.2373×10^{-5}	0.97889
BS1-Sr10 (10)	240	$y=-5.3071\times10^{-6}x$ -3.6618	-5.3071×10^{-6}	0.85487
BS1-Sr10 (10)	480	$y=-1.1108\times10^{-5}x$ -3.66124	-1.1108×10^{-5}	0.91353
BS1-Sr20 (20)	240	$y=-3.6276\times10^{-6}x$ -3.66166	-3.6276×10^{-6}	0.84535
BS1-Sr20 (20)	480	$y =-1.01511\times10^{-5}x$ -3.66115	-1.01511×10^{-5}	0.74657

The experiment was carried out at 240 rpm in the absence of additives, yielding a calculated reaction rate value $1.2373.10^{-5}$ min^{-1}, which corresponded very well with previously reported results in which order values of 5×10^{-3} and 2×10^{-2} were typically followed by barium sulfate crystallization [11]. Then, at a stirring speed of 480 rpm, the rate constant of barium sulfate precipitation from the solution rose somewhat. Furthermore, the calculated reaction rate constants might be used to estimate the effect of Sr-ions on the bulk precipitation of barium sulfate (Table 1).

As the concentration of Sr-ion increased, the reaction rate constant appeared to change. Based on the data presented above, a trace of Sr-cation might impede the production of barium sulfate crystals. On the other hand, increasing the stirring rate could accelerate the production of barium sulfate crystals, allowing for additional Sr-cation (20 ppm) to be virtually absorbed. Thereby, with faster stirring rate, the faster the nucleation rate of scale formation. In the same way, the stirring speed in a batch crystallization system was critical to the process's performance; it had to be sufficient to achieve the proper homogeneity of the two phases (solution and precipitate) and to keep up the suspension of solid particles. The results revealed that the highest barium sulfate crystal deposition rate, was obtained at the stirring speed of 480 rpm. This conclusion was consistent with the study's findings [29], which revealed that speeds greater than 400 rpm eliminated a significant amount of Sr coprecipitation with barium sulfate from the solution.

Furthermore, first-order reaction kinetics were used to evaluate the relationship between the influence of Fe^{3+}-ion and stirring speed (rpm) on the crystallization product of barium sulfate crystals (Table 2), and the estimated rates corresponded with the data previously reported [30]. Based on the results, varying reaction rates of barium sulfate products could be detected by Fe-cation. However, the increased rate might be attributed to the increase of its stirring speeds. Contrary to the similar results for the Fe-effect, Fe^{3+} co-precipitates with barium sulfate through adsorption processes [11], demonstrating that less barium sulfate crystal was precipitated at faster stirring speeds than when Fe-cation was added.

Table 2. Reaction rate constants for barium sulfate crystallization with Fe^{3+} cations.

Brines with Fe^{3+} (ppm)	Stirring rate (rpm)	Regression	Rate constant (k, M min-1)	R^2
BS1-Fe0 (0)	240	$y = -1.2802\times10^{-5}x$ -3.66129	-1.2802×10^{-5}	0.91353
BS1-Fe0 (0)	480	$y = -1.3625\times10^{-5}x$ -3.66126	-1.3625×10^{-5}	0.8744
BS1-Fe10 -10	240	$y = -8.9406\times10^{-6}x$ -3.6613	-8.9406×10^{-6}	0.81834
BS1-Fe10 -10	480	$y = -1.1866\times10^{-5}x$ -3.66128	-1.1866×10^{-5}	0.81946
BS1-Fe20 -20	240	$y = -8.2928\times10^{-6}x$ -3.66127	-8.2928×10^{-6}	0.8222
BS1-Fe20 -20	480	$y = -9.7531\times10^{-6}x$ -3.66133	-9.7531×10^{-6}	0.81536

XRD study of barium sulfate crystal

The XRD method based on the automated search-match processes was required to validate the crystallized barium sulfates qualitatively taken from the solution in the absence and the presence of additives. In accordance with the Crystallography Open Database (COD) card number #9014889, the phase identification of all measured XRD data indicated the single phase of barium sulfate (barite) crystallized at the stirring speeds (240 and 480 rpm) [31] could be obtained. Moreover, the XRD-Rietveld method [32] refined this crystal structure data, yielding the best refinement plot between the observed and calculated data, as shown in Fig. 5, for the BS0-sample. In the current investigation, a single phase of barite was formed regardless of Sr-cation concentrations or stirring speeds. For instance, no more peaks could be observed for other samples (Fig. 5a). The Sr^{2+} concentrations did not affect the makeup of the precipitate phases that had been collected. As a result, the minerals producing a solid solution precipitates could be obtained as the combination of any single crystal.

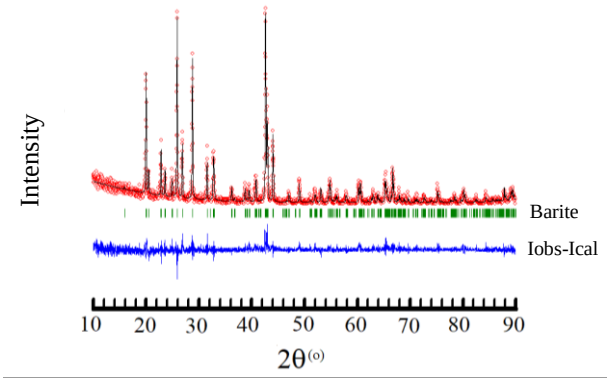

Fig. 5. XRD Rietveld analysis of BS0-sample without additives.

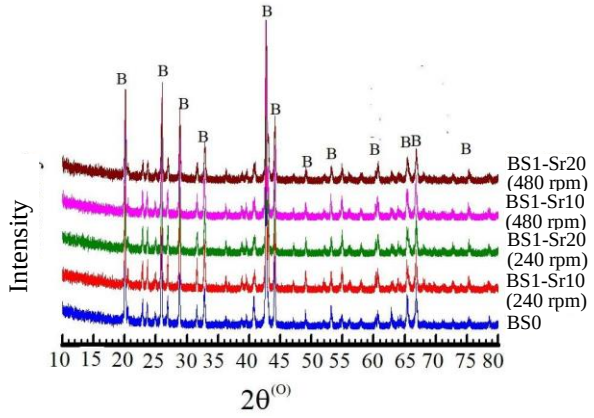

Fig. 5a. X-ray diffractograms of barium sulfate (B) precipitated without and with Sr-ions in BS0. BS1-Sr10. and BS1-Sr20 samples with various stirring rates are shown (rpm).

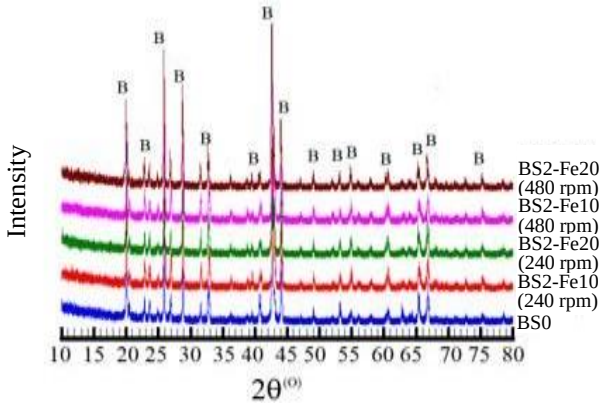

Fig. 5b. X-ray diffractograms of barium sulfate (B) precipitated without and with Fe-ions in BS0. BS2-Fe10. and BS2-Fe20 samples with various stirring rates are shown (rpm).

Moreover, as shown in Fig. 5b, the Rietveld XRD data method was used to validate BS0, BS2-Fe10, and BS2-Fe20 brine specimens containing pure barite. Based on the crystal structure data consistent with the reported investigation [32], it could produce barite crystals. The similar crystal structure of barite by increasing the iron (III) (10 and 20 ppm) and stirring speeds was also investigated by further research of XRD data for all specimens of (240 and 480 rpm).

On the contrary, barium sulfate could be seen in the X-ray diffraction patterns of several barium sulfate precipitates, which contained strontium and ferric ions. Furthermore, the improved lattice parameters and unit cell volumes of several barium sulfate crystals determined that the XRD Rietveld method could be performed, as shown in Table 3. Because Sr^{2+} ions had nearly equal ionic radii to barium ions, 1.13Å, and 1.34 Å, respectively, the lattice parameters of strontium-doped barium sulfate might remain unchangable if one Sr^{2+} was replaced by one Ba^{2+}. On the other hand, the ionic radius of ferric ions was substantially showed lower than that of barium (0.64Å for Fe^{3+} against 1.34 Å for Ba^{2+}). When Fe^{3+} ions were reacted with the barium sulfate lattice, the lattice properties would change insignificantly. Table 4 clearly showed that the lattice properties of the ferric iron-doped precipitates showed no trend. Any modification falls within the expected range of uncertainty; however, only a change in lattice volume could be detected in the BS2-Fe20 specimen when 20 ppm Fe^{3+} was injected.

Table 3. The $BaSO_4$ lattice parameters precipitated in the absence and presence of Sr^{2+} cation from the Rietveld XRD method.

Specimen	BS1-Sr0	BS1-Sr10 (240 rpm)	BS1-Sr20 (240 rpm)	BS1-Sr10 (480 rpm)	BS1-Sr20 (480 rpm)
a (Å)	8.8742(3)	8.8802(2)	8.8799(2)*	8.8836(2)	8.8795(6)
b (Å)	5.4582(5)	5.4529(4)	5.4517(4)	5.4516(4)	5.4562(6)
c (Å)	7.1590(7)	7.1560(4)	7.1568(5)	7.1561(5)	7.1582(8)
α	90	90	90	90	90
β	90	90	90	90	90
γ	90	90	90	90	90
V/ 10^6 pm3	346.758	346.51	346.469	346.566	346.803

Table 4. The $BaSO_4$ lattice parameters precipitated in the absence and presence of Fe^{3+} cation from the Rietveld XRD method.

Specimen	BS2-Fe0	BS2-Fe10 (240rpm)	BS2-Fe20 (240rpm)	BS2-Fe10 (480 rpm)	BS2-Fe20 (480 rpm)
a (Å)	8.8742(3)	8.8831(2)	8.8839(3)*	8.8813(3)	8.8822(2)
b (Å)	5.4582(5)	5.4538(4)	5.4550(4)	5.4525(4)	5.4516(3)
c (Å)	7.1590(7)	7.1581(5)	7.1614(5)	7.1571(5)	7.1540(4)
α	90	90	90	90	90
β	90	90	90	90	90
γ	90	90	90	90	90
V (Å)^3	346.758	346.79	347.05	346.584	346.416

Meanwhile, no definitive conclusions could be derived from the data. However, the results

were consistent with the predicted effects of ferric iron ions in the lattice. The matching diffraction patterns were given, as shown in Fig. 5b. For comparison. Although no new lines could be detected, changes in their relative strengths could be seen in ferric iron-containing precipitates. As a result, the iron-doped precipitates might generate patterns with considerably varying relative intensities, as shown in Fig. 5b.

Crystal morphology of barium sulfate

The precipitation conditions of an ionic solid were regarded to impact the appearance or behavior of the crystals formed substantially. It was well established that foreign ions could change the crystal behavior [33,34]. It was previously observed that foreign ions were mixed crystals of the precipitates, causing definite changes in habit modification. In contrast, ions just adsorbed onto the crystal surface did not induce significant changes to inhabit [5,35].

The typical form of barium sulfate precipitated in the absence of additives is depicted in Fig. 6a. SEM examination of the form of the precipitated barium sulfate crystals revealed the morphology of the characteristic rectangular tablets. Barium sulfate crystals precipitated from mixed brines had an average size of about 2.5 µm. However, as was shown in the SEM micrograph, the presence of additives altered the crystal habit of precipitated barium sulfate crystals. In the presence of strontium ions, the results were spherical tablets or flower-like clusters of tablets. However, increasing the stirring rate from 240 to 480 rpm resulted in as-prepared flower-like aggregates composed of several spherical tablets that developed randomly from the center of a given mother tablet (Figs. 6c-d). If stirred faster, the crystals would form a spherical tablet shape. An increased stirring rate of barium sulfate crystallization resulted in the regulated aggregation or growth of flower-like aggregate particles, yielding particles with an average size of 5mm (Fig. 6e).

Moreover, strontium ions had a more obvious effect than ferric ions. An SEM image of $BaSO_4$ crystals precipitated in the presence of ferric ions is shown in Fig. 7. Fe (III) concentrations in this solution were comparable to the amounts of strontium ions in the solution from which the crystals in Fig. 6b were formed. However, sediments formed by ferric iron ions from $FeCl_3$ (solubility in water: 920 g/l at 20 °C) produce a smaller aggregate of crystals. They are nif.early distinct from precipitates without Sr^{2+} and Fe^{3+} ions [36,37].

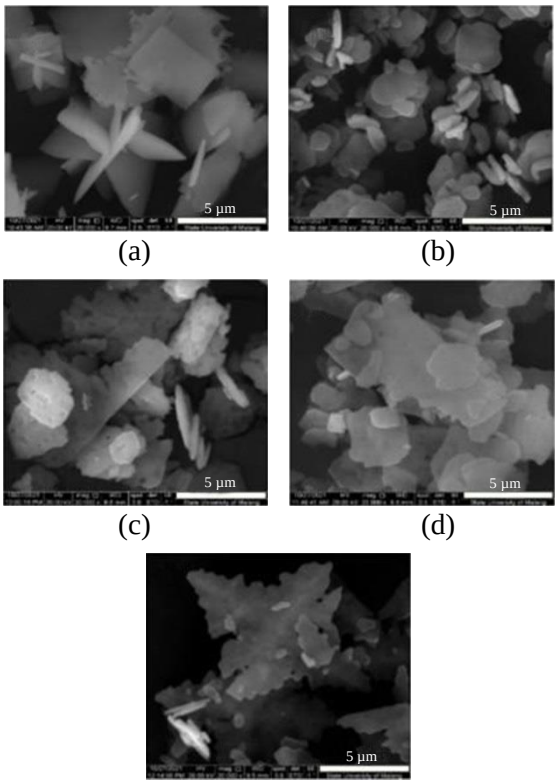

Fig. 6. SEM Micrographs of barium sulfate crystals in the presence of Sr ions for samples; a) BS0, 240 rpm; b) BS1-Sr10, 240 rpm; c) BS1-Sr10, 480 rpm; d) BS1-Sr20, 240 rpm; e) BS1-Sr20, 480 rpm.

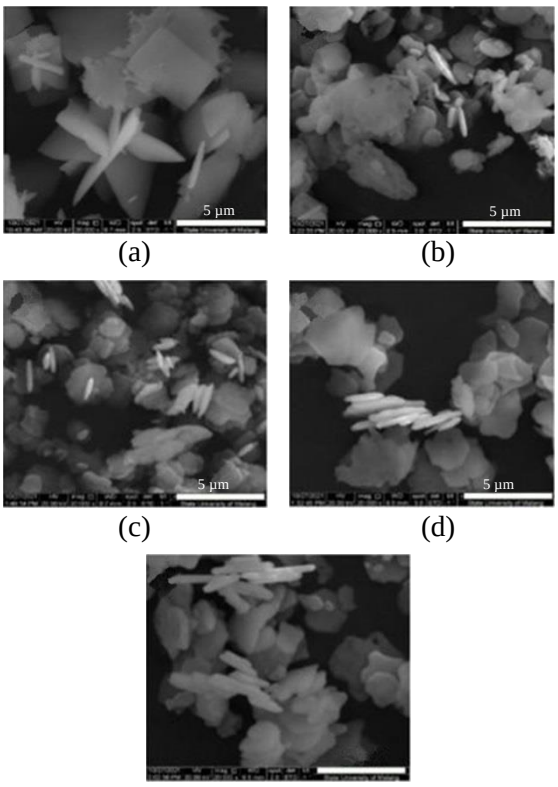

Fig. 7. SEM Micrographs of barium sulfate crystals in the presence of Fe- ions a) BS0, 240 rpm; b) BS2-Fe10, 240 rpm; c) BS2-Fe10, 480 rpm; d) BS2-Fe20, 240 rpm; e) BS2-Fe20, 480 rpm.

Apart from that case, the effect of ferric iron on morphology could be studied with a different approach. When both Sr^{2+} and Fe^{3+} ions were added in the solution, the crystal habit of the resulting precipitate (Fig. 6d) would change the way that corresponds with Sr^{2+} ions, corresponding to $SrCl_2$ solubility being greater than that of $BaCl_2$ (Fig. 6b). Still, the change in crystal habit due to strontium ions was less pronounced when ferric iron was also present in solution [19,38].

The ANOVA parameters is shown at Table 5. At the 0.05 level, the population means of $SrCl_2$ inhibitor concentration are significantly different. At the 0.05 level, the population means of stirring rate are also significantly different. At the 0.05 level, the interaction berween $SrCl_2$ inhibitor concentration and stirring rate is not significantly different [39].

Table 5. Results of ANOVA for Barium Sulfate crystallization yield.

Source	Degrees of freedom	Sum of Squares	Mean Square	F Value	P Value
Model	5	$7{,}21597\times10^{-4}$	$1{,}44319\times10^{-4}$	6,66495	0.00112
$SrCl_2$ inhibitor concentration	2	$5{,}30606\times10^{-4}$	$2{,}65303\times10^{-4}$	12,25221	$4{,}38072\times10^{-4}$
Stirring rate	1	$1{,}7876\times10^{-4}$	$1{,}7876\times10^{-4}$	8,25551	0.01011
Interaction	2	$1{,}22308\times10^{-5}$	$6{,}11542\times10^{-6}$	0.28242	0.75724
Error	18	$3{,}89763\times10^{-4}$	$2{,}16535\times10^{-5}$	---	---
Corrected Total	23	0.00111	---	---	---

CONCLUSION

The experimental results showed that as the mass precipitation of barium sulfate decreased in the presence of strontium and ferric iron, pure barite was formed in the synthetic brine experimental conditions. Furthermore, no change in phase composition of barite was observed in the presence of strontium, ferric iron, or stirring rates. The morphology of barite was demonstrated using SEM micrographs, which showed primarily tablet-shaped crystals and fewer crystals with tubular shapes. However, in this particular case, a generic reaction rate equation for barium sulfate precipitation from the reservoir for a specific brine, supersaturation, and mixing time durations could be determined.

AUTHOR CONTRIBUTION

Conceptualization, investigation & data curation, S.Susilowati and Novel Karaman; project administration, original draft preparation, S.Susilowati and D.Thagrina Aruba; Analysis, visualization, S.Susilowati, Novel Karaman, and A.Rama Prayuga; writing, editing, A.Rama Prayuga, D. Thagrina Aruba, Sukirmiyadi and Lilik Suprianti. All authors have read and agreed to the published version of the manuscript

REFERENCES

1. M. Boon and F. Jones, Cryst. Growth Des. **16** (2016) 4646.
2. A. Shabani, A. Kalantariasl, M. Parvazdavani, *et al.*,, J. Pet. Sci. Eng. **176** (2019) 1071.
3. M. S. Kamal, I. Hussein, M. Mahmoud *et al.*, J. Pet. Sci. Eng. **171** (2018) 127.
4. M. M. Vazirian, T. V. J. Charpentier, M. D.O. Penna *et al.*, J. Pet. Sci. Eng. **137** (2016) 22.
5. H. E. Gomaa, A. A. Alotaibi, F. A. Gomaa *et al.*, Process Saf. Environ. Prot. **153** (2021) 500.
6. A. Shabani, H. Sisakhti, S. Sheikhi *et al.*, J. Pet. Sci. Eng. **190** (2020) 107031.
7. M. S. H. Bader, J. Pet. Sci. Eng. **55** (2007) 93.
8. A. B. BinMerdhah, A. A. M. Yassin and M. A. Muherei, J. Pet. Sci. Eng. **70** (2010) 79.
9. I. H. Widanagamage, A. R. Waldron and M. Glamoclija, Minerals **8** (2018) 480.
10. G. H. Nancollas and S. T. Liu, SPE J. **15** (1975) 509.
11. F. Jones, M. I. Ogden and T. Radomirovic, J. Cryst. Growth **498** (2018) 148.
12. E. Akyol, Ö. Aras and M. Öner, Desalin. Water Treat. **52** (2014) 5965.
13. E. Smith, J. Hamilton-Taylor, W. Davison *et al.*, Chem. Geol. **207** (2004) 81.
14. B. S. Bageri, M. A. Mahmoud, R. A. Shawabkeh *et al.*, Arab. J. Sci. Eng. **42** (2017) 1667.
15. O. Ephraim and U. Awajiogak, Int. J. Eng. Res. Appl. **6** (2016) 62.
16. A. Al-Othman, N. N. Darwish, M. Qasim *et al.*, Desalination **457** (2019) 39.
17. H. Gamal, S. Al-Afnan, S. Elkatatny *et al.*, Geofluids **2021** (2021) 1
18. M. A. Kelland, Ind. Eng. Chem. Res. **50** (2011) 5852.
19. F. Jones, A. Oliveira, A. L. Rohl *et al.*, J. Cryst. Growth **237** (2002) 424.

20. A. Khormali, G. Bahlakeh, I. Struchkov *et al.*, J. Pet. Sci. Eng. **202** (2021) 108589.

21. I. H. Widanagamage, E. A. Schauble, H. D. Scher *et al*., Geochim. Cosmochim. Acta **147** (2014) 58.

22. A. Altomare, C. Cuocci, C. Giacovazzo *et al.*, J. Appl. Crystallogr. **41** (2008) 815.

23. J. Rodriguez-Carvajal, Full Prof 2000 (2021).

24. S. Gražulis, D. Chateigner, R. T. Downs *et al.*, J. Appl. Crystallogr. **42** (2009) 726.

25. P.-Y. Mahieux, J.-E. Aubert, M. C. M. Coutand *et al*,.Waste Manage. **30** (2010) 378.

26. G. Ivanto, F. Fatra, N. S. Dera *et al.,* IOP Conf. Ser. Mater. Sci. Eng. **202** (2017) 012015.

27. D. S. Perwitasar, S. Muryanto, J. Jamari *et al.*, Cogent Eng. **9** (2022) 1.

28. S. Raharjo, Buku Referensi: Pembentukan dan Pengendalian Kerak Mineral di dalam Pipa, (2020) 1. (in Indonesian)

29. J.-G. Cao, P. Gu, J. Zhao *et al.*, J. Radioanal. Nucl. Chem. **285** (2010) 539.

30. F. Jones, A. Oliviera, G. M. Parkinson *et al.*, J. Cryst. Growth **262** (2004) 572.

31. A. I. Ebunu, Y. A. Olanrewaju, O. Ogolo *et al*., Heliyon **7** (2021) 1.

32. S. M. Antao, Am. Mineral. **97** (2012) 661.

33. E. Aboelezz, C. De Angelis and P. Fattibene, Measurement **175** (2021) 109108.

34. R. B. Fischer and R. B. Rhinehammer, Anal. Chem. **25** (1953) 1544.

35. A. G. Walton, H. Füredi, P. J. Elving *et al.*, The Formation and Properties of Precipitates, Interscience Publishers New York (1967).

36. L. Li, Z. Yan, X. He *et al.,* Colloids Surfaces., A, **631** (2021) 127668.

37. B. Sadeghalvad, N. Khorshidi, A. Azadmehr *et al*., Chemosphere **263** (2021) 128064.

38. S. Charles, D. W. Bui, T. Canler *et al.*, Forensic Sci. Int. **331** (2022) 111127.

39. L. Sthle and S. Wold, Chemom. Intell. Lab. Syst. **6** (1989) 259.